Geophysical Research Letters

RESEARCH LETTER
10.1029/2025GL114658

Causes of the Abnormally Strong Easterly Phase of the Mesopause Semiannual Oscillation During the March Equinox of 2023 Revealed by a New Reanalysis Data Covering the Entire Middle Atmosphere

Kaoru Sato[1], Dai Koshin[2], Jose Suclupe[3], Jorge L. Chau[3], Lourivaldo M. Lima[4], Guozhu Li[5], S. Vijaya Bhaskara Rao[6], M. Venkat Ratnam[7], Rodolfo Rodriguez[8], and Danny Scipion[9]

[1]Department of Earth and Planetary Science, The University of Tokyo, Tokyo, Japan, [2]High Altitude Observatory, NSF National Center for Atmospheric Research, Boulder, CO, USA, [3]Leibniz-Institute of Atmospheric Physics at the University of Rostock, Kühlungsborn, Germany, [4]Universidade Estadual da Paraiba, Campina Grande, Brazil, [5]Beijing National Observatory of Space Environment, Institute of Geology and Geophysics, Chinese Academy of Sciences, Beijing, China, [6]Department of Physics, Sri Venkateswara University, Tirupati, India, [7]National Atmospheric Research Laboratory, Tirupati, India, [8]Universidad de Piura, Piura, Peru, [9]Radio Observatorio de Jicamarca, Instituto Geofisico del Peru, Lima, Peru

Abstract During the March equinox of 2023, a strong easterly wind of ∼80 m s^{-1} appeared at an altitude of ∼82 km in the equatorial upper mesosphere, which is regarded as an enhancement of the mesopause semi-annual oscillation. In this study, a new reanalysis data available up to 110 km was used to investigate its momentum budget. The strong easterly acceleration was due to a similar contribution from resolved waves and parameterized gravity waves, but largely counteracted by an upward advection of westerly momentum. The significant anomaly in the mean winds was not restricted to the 82 km height, but also included strong westerly winds (∼50 m s^{-1}) at 65 km and easterly winds (∼40 m s^{-1}) at 42 km. The stratospheric quasi-biennial oscillation was westerly. The mean wind intensification at each height is explained by the acceleration due to upward propagating waves, which do not suffer from critical filtering below.

Plain Language Summary In March 2023, a strong easterly wind (around 80 m s^{-1}) was observed at an altitude of 82 km in the equatorial upper mesosphere, indicating a strengthening of the mesopause semi-annual oscillation (SAO). Using a new data up to 110 km, this study analyzed the forces driving this wind. The strong easterly wind was caused equally by both large-scale waves and subgrid-scale waves such as gravity waves, but this effect was largely offset by the upward movement of westerly momentum. Unusual wind patterns were also seen at lower heights: strong westerly winds (∼50 m s^{-1}) at 65 km and strong easterly winds (∼40 m s^{-1}) at 42 km. The quasi-biennial oscillation showed westerly phase. The wind intensification at these altitudes can be explained by upward propagating waves, which do not suffer from filtering below.

Key Points:

- A new reanalysis up to 110 km was used to examine the cause of the equatorial strong easterly winds at 82 km around March equinox 2023
- Critical level filtering of eastward waves below the strong westerly winds at 65 km likely enhances westward forcing at 82 km
- This westward forcing is much larger than the zonal wind tendency and is largely counteracted by the upward zonal wind advection

Supporting Information:

Supporting Information may be found in the online version of this article.

Correspondence to:

K. Sato,
kaoru@eps.s.u-tokyo.ac.jp

Citation:

Sato, K., Koshin, D., Suclupe, J., Chau, J. L., Lima, L. M., Li, G., et al. (2025). Causes of the abnormally strong easterly phase of the mesopause semiannual oscillation during the March equinox of 2023 revealed by a new reanalysis data covering the entire middle atmosphere. *Geophysical Research Letters*, *52*, e2025GL114658. https://doi.org/10.1029/2025GL114658

Received 15 JAN 2025
Accepted 4 MAR 2025

Author Contributions:

Conceptualization: Kaoru Sato
Data curation: Kaoru Sato, Jose Suclupe, Jorge L. Chau, Lourivaldo M. Lima, Guozhu Li, S. Vijaya Bhaskara Rao, M. Venkat Ratnam, Rodolfo Rodriguez, Danny Scipion
Formal analysis: Kaoru Sato, Dai Koshin
Funding acquisition: Kaoru Sato
Methodology: Kaoru Sato
Resources: Kaoru Sato
Validation: Kaoru Sato
Writing – original draft: Kaoru Sato
Writing – review & editing: Dai Koshin, Jose Suclupe, Jorge L. Chau, Lourivaldo

1. Introduction

An extremely strong easterly (westward) zonal wind with a speed of −80 m s^{-1} at an altitude of z = 82 km was observed in the tropics by multiple meteor radars around the equinox of March 2023. This phenomenon is regarded as an intensification of the easterly phase of the equatorial mesopause semiannual oscillation (M-SAO) (Suclupe et al., 2024). The M-SAO is an semi-annual oscillation (SAO) in the zonal mean zonal wind in the height range of 65–100 km, with a peak at z = ∼80 km (e.g., Hirota, 1978). Moreover, two distinct types of large-scale oscillations in the zonal mean zonal wind are present below the M-SAO region, which are considered to be closely related to the M-SAO. The stratopause SAO (S-SAO) is observed in the height region of 30–55 km with a peak at z = ∼50 km (e.g., Reed, 1966). The S-SAO exhibits a phase difference of 180° with respect to the M-SAO. The existence of these SAOs was initially identified through rocket sonde data, and subsequent observations by High Resolution Doppler Interferometer (HRDI) onboard the Upper Atmosphere Research Satellite (UARS) provided further confirmation (Garcia et al., 1997). These observations indicated that the easterly winds associated with both the S-SAO and M-SAO exhibited enhanced strength during the first cycle, which corresponds to the December solstice for the S-SAO and the March equinox for the M-SAO. Furthermore, a significant interannual variability has been documented. Moreover, a notable interannual oscillation called the quasi-biennial oscillation

M. Lima, Guozhu Li, S. Vijaya Bhaskara Rao, M. Venkat Ratnam, Rodolfo Rodriguez, Danny Scipion

(QBO) is observed between 17 and at least 40 km in the stratosphere (Smith et al., 2017). The oscillatory period is ∼28 months. A common feature of these oscillations is that the phase descends with time, although the descent rate varies depending on the phase of each oscillation and may not be much noticeable.

An important driving mechanism of these large-scale oscillations is the forcing caused by upward propagating waves interacting with the mean zonal flow. When a wave approaches its critical level in which the difference between the phase speed and the mean wind becomes small, non-conservative processes tend to occur below the critical level (e.g., Andrews et al., 1987): For example, the wave breaking occurs as the amplitude of horizontal wind and temperature fluctuations associated with the wave increases and the vertical wavelength shortens. In addition, the upward group velocity is reduced and the wave is attenuated by radiative relaxation. The wave forcing generated from these nonconservative processes accelerates or decelerates the mean wind to the wave phase speed below the critical level. As a result, the phase of the oscillation descends with the wave forcing. Another mechanism that does not necessarily involve phase descent is westward forcing associated with Rossby wave breaking from mid to high latitudes. Wave forcing also occurs in the absence of the critical layer. As the air density decreases with height, the horizontal wind and temperature wave amplitudes increase with height, and wave breaking tends to occur at higher altitudes. This process should be more effective at higher levels, as supported by satellite observations in the upper mesosphere (Ern et al., 2021). The westward forcing not only causes easterly acceleration directly, but also indirectly induces easterly acceleration in the equatorial region by driving poleward residual flows and transporting angular momentum poleward from the equator (Delisi & Dunkerton, 1988; Holton & Wehrbein, 1980). In the event that the residual flows originating from the opposite hemisphere extend across the equator, the flow causes a more pronounced acceleration of easterly winds at the equator (Tomikawa et al., 2008).

For the QBO, it is considered that westerly acceleration is predominantly caused by gravity waves (GWs) and equatorial Kelvin waves with eastward phase speed, whereas easterly acceleration is primarily due to GWs with westward phase speed, and secondarily due to Rossby-gravity waves (e.g., Baldwin et al., 2001). The S-SAO is considered to be driven by westerly acceleration due to fast equatorial Kelvin waves, which do not contribute to the QBO (Hirota, 1978; Hitchman & Leovy, 1988), and direct and indirect easterly acceleration by westward forcing by quasi-stationary Rossby waves from higher latitudes (Holton & Wehrbein, 1980). The additional contribution by GWs is indicated to either easterly or westerly acceleration (Antonita et al., 2008; Ray et al., 1998). The M-SAO driving processes, as suggested by previous studies, comprise westerly acceleration by faster equatorial Kelvin waves, westerly and easterly acceleration by GWs selectively transmitted through the mean zonal winds of the QBO and S-SAO, and easterly acceleration by tides (Ern et al., 2021; Garcia, 2023; Suclupe et al., 2024). The close relation between the QBO and S-SAO was documented by Smith et al. (2017).

Both SAO and QBO are climatologically important phenomena, influencing not only zonal mean zonal winds but also temperature, ozone, and other substances (Smith et al., 2023). Moreover, their interaction with large-scale variability at mid- and high-latitudes is also notable, affecting surface climate (Gray et al., 2022). With regard to the S-SAO, the use of reanalysis data that have been assimilated with long-term observations from satellites such as the Sounding of the Atmosphere using Broadband Emission Radiometry (SABER) and the Microwave Limb Sounder (MLS) has great potential to elucidate the detailed mechanism, although there are non-negligible discrepancies between reanalysis data sets (Kawatani et al., 2020). Model intercomparison for the S-SAO shows consistent results among models (Smith et al., 2020). However, requisite reanalysis data for the M-SAO had not been available until recently, thereby rendering it challenging to study its spatial structure and momentum budget. In this study, recently produced reanalysis data, JAWARA (Koshin et al., 2025; Sato, 2025), covering the entire neutral atmosphere up to 110 km, are employed to examine the structure of the extreme easterly event in the March equinox season in 2023 and its dynamics, with comparison made with the condition in the same season in 2022.

2. Data Description

2.1. A New Reanalysis Data, JAWARA, Covering the Entire Neutral Atmosphere

JAWARA used in this study is a new hourly reanalysis data set for the entire neutral atmosphere from the surface up to z = 110 km, currently covering ∼20 years from 2004 to 2024 (Koshin et al., 2025; Sato, 2025). The time period from January 2022 to September 2023, including the notable easterly wind event around the March equinox of 2023, is mainly examined. JAWARA was produced from a recently developed data assimilation

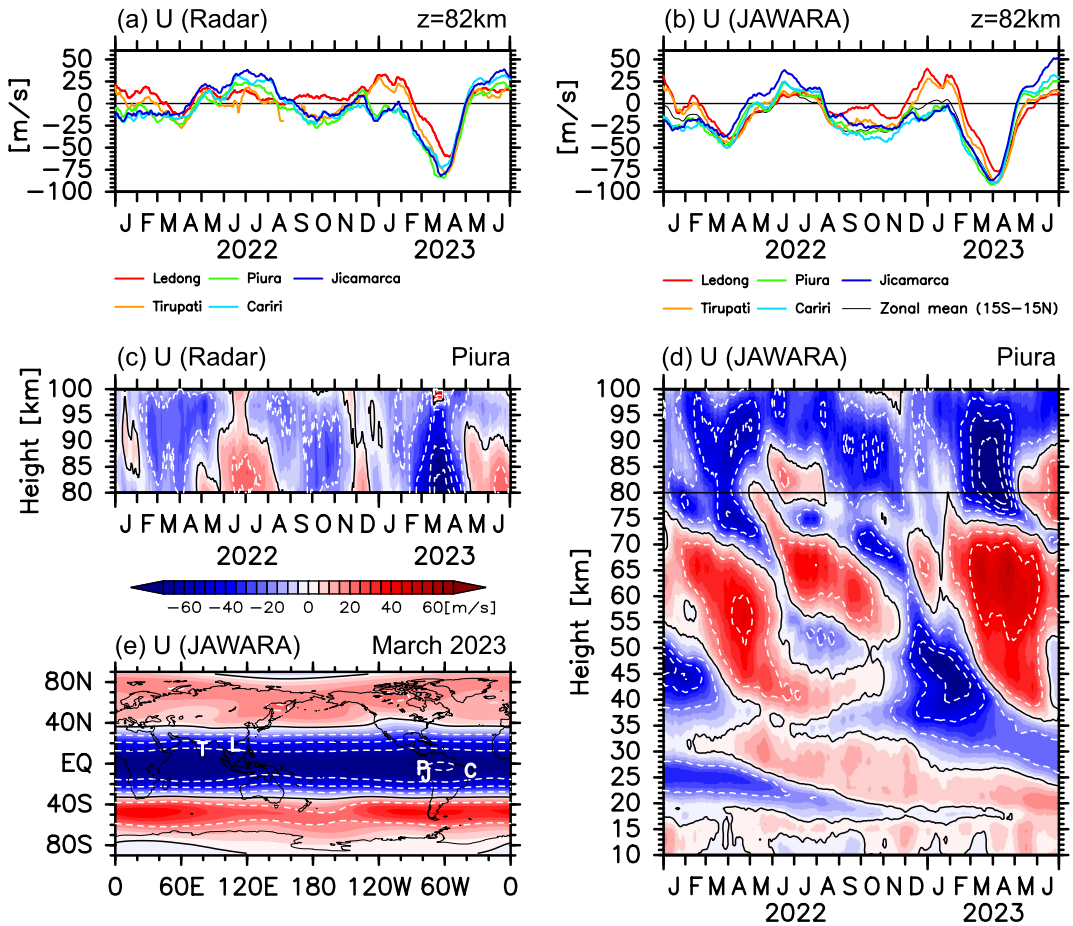

Figure 1. Time series of the zonal wind at Ledong (18.4°N, 109.0°E), Tirupati (13.6°N, 79.4°E), Piura (5.5°S, 80.4°W), Cariri (7.4°S, 36.5°W), and Jicamarca (11.9°S, 76.8°W) (a) from meteor radars and (b) JAWARA. Time-height section of the zonal wind at Piura: (c) the meteor radar and (d) JAWARA. (e) A horizontal map of the zonal wind at z = 82 km in March 2023. The location of each station is denoted by the initial letter of its name.

system using a high-top general circulation model, called the Japanese Atmospheric General circulation model for Upper Atmosphere Research Data Assimilation System (JAGUAR-DAS, Koshin et al., 2020, 2022). JAWARA is an abbreviation of the JAGUAR-DAS Whole neutral Atmosphere ReAnalysis. An intercomparison of middle atmospheric analyses by McCormack et al. (2021) showed that JAWARA, of sufficient quality, is comparable to other state-of-the-art reanalysis data. See Koshin et al. (2025) for details on JAWARA.

2.2. Meteor Radar Data

Suclupe et al. (2024) first described the strong easterly wind event during the March equinox of 2023 using hourly horizontal winds from five meteor radars. The radars are located at Jicamarca (11.9°S, 76.8°W) (Chau et al., 2021; Suclupe et al., 2023) and Piura (5.5°S, 80.4°W) (Conte et al., 2023; Poblet et al., 2023) from Spread Spectrum Interferometric Multistatic Meteor Radar Observing Network (SIMONe), and at Cariri (7.4°S, 36.5°W) (Buriti et al., 2008), Tirupati (13.6°N, 79.4°E) (Rao et al., 2014), and Ledong (18.4°N, 109.0°E) (Wang et al., 2019). The temporal and vertical resolutions of the radar data are 1 hr and 2 km, respectively. The height range is from 80 to 100 km. These radar data were used to validate the reproductivity of the event in JAWARA.

3. Results

3.1. Comparison of JAWARA With Meteor Radar Data

Figure 1a represents the time series of zonal winds from meteor radars at five stations from January of 2022 to June of 2023 at z = 82 km. A 21-day running mean is applied to represent a more representative overview of the

data. The zonal winds display semi-annual variations which are prevailingly easterly during equinoctial periods and westerly during solstitial ones. The time period encompasses two March equinoxes in 2022 and 2023, which exhibit markedly different easterly winds. In 2023, the easterly winds are strong, reaching the speed of -80 m s^{-1} at most stations, except for Ledong, located at the highest latitude. In contrast, the easterly wind is only ~-20 to -30 m s^{-1} in 2022. The westward acceleration is large from the beginning of February through the end of March in 2023. Figure 1b shows the time series of zonal winds at respective radar stations from JAWARA which the same running mean was applied to. JAWARA well reproduces both strong easterly winds of the 2023 March equinox and the weak ones of 2022 including the differences among stations, though slightly over-estimated.

Figures 1c and 1d show the time-height sections of zonal winds at Piura from radar and JAWARA, respectively. Although there is westward bias in JAWARA, most features in the semi-annual variation are well reproduced, such as stronger easterly winds during the March equinoctial season than during the September one, and stronger westerly winds during the June solstitial season than during the December one. JAWARA also well captured the difference in the vertical structure of the March-equinoctial easterly winds between 2022 and 2023: The easterly wind is minimized at $z = \sim$80 km in 2022, while it is maximized there in 2023. Comparisons for other radar sites are given as Figure S1.

The JAWARA time-height section (Figure 1d) covers a wide height range of z = 10–100 km. A notable discrepancy is observed around the March equinox between 2022 and 2023 also regarding the strength of westerly winds for z = 40–72 km, that is considerably stronger in 2023. The westerly maximum in 2023 is located at $\sim$65 km. Additionally, strong easterly winds are observed above $z = \sim$35 km in 2023 than those in 2022 during the March equinox. The stratospheric QBO is observed below z = 35 km. The QBO phase differs between the two years, with an easterly phase in 2022 and a westerly phase in 2023 at $z = \sim$25 km. As discussed later, these differences are considered a key that causes the difference in the March equinoctial easterly winds around z = 82 km between the 2 years.

Figure 1e shows a horizontal map of zonal wind averaged for March 2023 at z = 82 km. The strong easterly wind is roughly zonally uniform with a slight maximum over the American continent. In terms of the latitude, the easterly wind is maximized on the equator, extending from 20°S to 20°N as a half width.

3.2. Momentum Budget Analysis

The transformed Eulerian-mean zonal momentum equation (e.g., Andrews et al., 1987) is used for the momentum budget analysis;

$$\frac{\partial \overline{u}}{\partial t} = \left[f - \frac{1}{a\cos\phi}\frac{\partial(\overline{u}\cos\phi)}{\partial\phi} \right]\overline{v}^* - \frac{\partial \overline{u}}{\partial z}\overline{w}^* + \frac{1}{\rho_0 a\cos\phi}\nabla\cdot\boldsymbol{F} + \overline{X}, \tag{1}$$

where

$$\overline{v}^* \equiv \overline{v} - \frac{1}{\rho_0}\frac{\partial}{\partial z}\left(\rho_0\frac{\overline{v'\theta'}}{\theta_{0z}}\right), \overline{w}^* \equiv \overline{w} + \frac{1}{a\cos\phi}\frac{\partial}{\partial\phi}\left(\cos\phi\frac{\overline{v'\theta'}}{\theta_{0z}}\right),$$

$$\boldsymbol{F} \equiv \left[0, \rho_0 a\cos\phi\left(\overline{u}_z\frac{\overline{v'\theta'}}{\theta_{0z}} - \overline{v'u'}\right), \rho_0\cos\phi\left(f - \frac{\partial(\overline{u}\cos\phi)}{\partial\phi}\frac{\overline{v'\theta'}}{\theta_{0z}} - \overline{w'u'}\right)\right].$$

Here, u, v, and w are zonal, meridional, and vertical wind components, respectively, θ is the potential temperature, a the Earth's radius, ρ_0 and θ_0 are the basic density and potential temperature, respectively, f is the Coriolis parameter, and ϕ and z are the latitude and log-pressure height, respectively. The residual mean flow $(\overline{v}^*, \overline{w}^*)$ is a good approximation to the Lagrangian-mean flow. The EP flux due to waves resolved in JAWARA is denoted by $\boldsymbol{F}$, while X represents unresolved waves such as small-scale GWs. The term X is partly expressed by the GW parameterizations, but it is imperfect. The effects of lateral propagation, transience, and secondary generation of GWs are not represented (e.g., Kim et al., 2024; Sato et al., 2009, 2012; Vadas et al., 2018), either. The deviation of true GW forcing from the parameterized GW forcing should be compensated by the assimilation increment in the reanalysis (Sato & Hirano, 2019).

To elucidate the cause of the extreme easterly wind event, a momentum budget analysis was performed at $z = 82$ km, where the easterly winds are maximized in early April 2023. Specifically, the first three terms on the right side of 1 and the parameterized GW forcing (GWFp) are examined and compared with the zonal wind tendency $\overline{u}_t$ on the left side of 1. The assimilation increment, which expresses possible unexpressed forcing, is also examined. Figure 2a shows the time series of $\overline{u}_t$, $\frac{1}{\rho_0 a \cos\phi}\nabla \cdot \boldsymbol{F}$ (EPFD), GWFp, and the total wave forcing (EPFD + GWFp). A largely negative $\overline{u}_t$ is observed in February and March 2023. The EPFD is largely negative in both months, whereas the GWFp is largely negative only in March. The sum of the wave forcings is considerably larger than $\overline{u}_t$ in March, while it is comparable to that in February. The EPFD in March 2022 is comparable to that in March 2023. Thus, the substantial total wave forcing in March 2023 is primarily attributed to the strong GWFp.

The EPFD is divided into tidal (TW) and non-tidal (non-TW) wave components, where the TW component represents the sum of three distinct types of waves: the migrating diurnal tide with zonal wavenumber 1 ($s = 1$), semi-diurnal tide with $s = 2$, and terdiurnal tide with $s = 3$ (Figure 2b). Note that Suclupe et al. (2024) suggested that TWs play a role in the occurrence of the strong easterly wind event. The negative EPFD in February 2023 is attributed primarily to the non-TW, whereas both TW and non-TW have a comparable contribution to the EPFD in March 2023.

The total negative wave forcing, that greatly exceeds $\overline{u}_t$, is almost canceled by the total positive angular momentum advection by the residual mean flow, $\left[f - \frac{1}{a\cos\phi}\frac{\partial(\overline{u}\cos\phi)}{\partial\phi}\right]\overline{v}^* - \frac{\partial\overline{u}}{\partial z}\overline{w}^*$, in March 2023 as in Figure 2c. Such positive advection is not observed in other time periods shown in Figure 2c. This zonal momentum advection is predominantly attributable to the vertical advection in March 2023, which is discussed in detail in Section 3.3. This substantial upward advection of the eastward momentum may prevent the downward propagation of the easterly phase of the M-SAO below $z = \sim$75 km, consistent with the feature in Figure 1d.

It is important to note that in March 2023, the total positive momentum advection (Figure 2c) is substantially stronger than the total negative wave forcing (Figure 2a), indicating a shortage of negative forcing for the momentum balance. Figure 2d shows the time series of the assimilation increment, which is significantly negative in March 2023, while exhibiting positive values in other time periods. This may be due to the limited assimilated observations above ~80 km, but also suggests unidentified processes in the model, such as lateral propagation, secondary generation, and transience of GWs, and/or imperfect representation of upward GWs in the parameterization.

3.3. Spatial Structure of Extreme Easterly Wind Event

In this section, we examine the mechanism of strong upward westerly momentum advection in terms of the residual mean flow and absolute angular momentum (AAM). Figures 3a and 3b show the meridional cross sections of the residual mean flows and their vertical components, overlaid with AAM contours for March 2022 and 2023, respectively. Figures 3c and 3d are similar to Figures 3a and 3b, but for the E-P flux and its divergence (EPFD), overlaid with the zonal mean zonal wind contours. Figures 3e and 3f show the same as Figures 3c and 3d, but for the GWFp.

The easterly winds are maximized near the equator with a latitudinal extension of 40° (i.e., 20°S to 20°N) as a half width for $z = \sim$80–105 km in 2023. This extension is wider than in 2022. Compared to 2022, the poleward residual mean flow in the Northern Hemisphere (NH) in 2023 is notably stronger above 75 km. As required by the continuity equation, this is accompanied by a strong upward residual flow in the tropics in $z = 70$–82 km, where the AAM vertical gradient is largely negative. The combination of the strong upward flow and the large AAM vertical gradient is the reason for the strong upward zonal momentum advection observed in Figure 2c.

This stronger poleward residual mean flow in 2023 is attributable to more largely negative GWFp in the NH midlatitudes than in 2022. The GWFp intensity difference between the two years can be attributed to the zonal wind structure in the NH. Only in 2023, the polar night jet is present even in March, which hinders upward propagation of GWs with faster zonal phase speed c_x facilitating eastward acceleration through their breaking in the upper atmosphere in the NH midlatitudes.

Notably, the EPFD above 84 km has a structure consistent with TWs. If the diurnal tide breaks with amplitude limited by saturation, the maximum acceleration should remain relatively unchanged (Garcia, 2023; Lindzen, 1981). The tide amplitude in 2023 exceeded that in 2022 (Suclupe et al., 2024), suggesting that acceleration

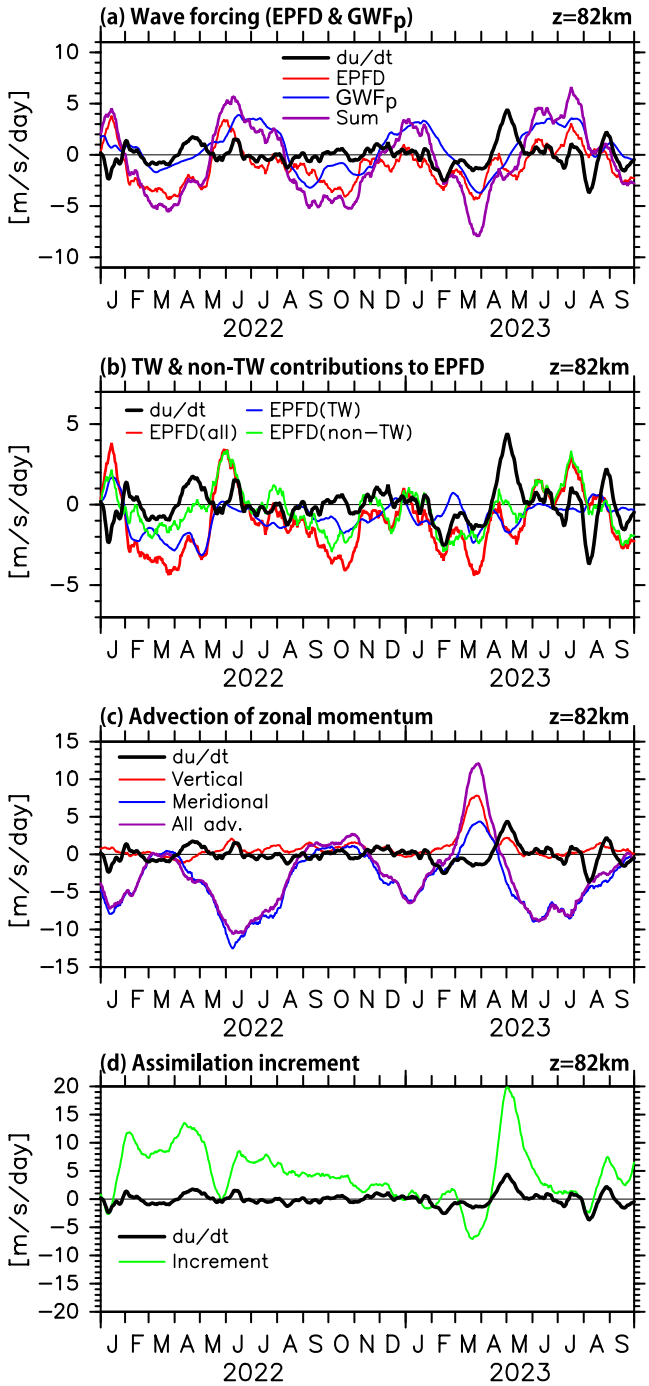

Figure 2. Time series of each component of the zonal mean zonal momentum equation, averaged over 15°S–15°N. (a) E-P flux divergence (EPFD) (red), parameterized gravity wave forcing (blue), and their sum (purple). (b) EPFD due to all waves (red), tidal waves (blue) and non-tidal waves (green). (c) Vertical (red) and meridional (blue) advections of the zonal momentum and their sum (purple). (d) The assimilation increment. The time series of the zonal mean zonal wind tendency is plotted by black curves in all figures.

starts from lower altitudes, consistent with Figures 3c and 3d. Furthermore, the greater latitudinal extent of tidal EPFD in 2023 than in 2022 aligns with the wider small $f - \overline{u}_y$ region, linked to the stronger and wider equatorial easterly winds.

3.4. Vertical Wave Filtering Related to the Vertical Structure of Mean Zonal Wind

As shown in Section 3.2, the westward wave forcing was enhanced in March 2023. To elucidate the underlying cause, the upward propagation of the waves is examined as a function of c_x. The upward propagating waves tend to accelerate the mean wind toward their phase speed through critical level absorption, radiative relaxation, and/or wave breaking. The mean flow acceleration by the wave breaking is more important at higher altitudes, due to the exponential increase in wave amplitude as a result of the exponential decrease in atmospheric density with height (e.g., Ern et al., 2021). Figure 4 represents vertical profiles of the zonal mean zonal wind $\overline{u}$ in March (thick curves) and April (thin curves) in 2022, 2023, and the climatology for 2005–2023 averaged over 15°S–15°N. Shaded are the c_x range of the waves that propagate upward through $z = 20$ km and do not reach their critical levels. In March 2023, notable strong mean winds other than the strong easterly wind at $z = \sim$82 km are observed compared with those in 2022 and the climatology: Strong westerly winds with a peak of ~50 m s^{-1} at $z = \sim$65 km and strong easterly winds with a peak of −40 m s^{-1} at $z = \sim$42 km.

In both 2022 and 2023, waves with $c_x < -80$ m s^{-1}, which are necessary to accelerate and form the easterly mean wind maximum of −80 m s^{-1}, can reach $z = 82$ km. A difference is observed in waves with positive c_x below. In 2023, due to the strong westerly wind at $z = \sim$65 km, the c_x range of eastward waves is narrower ($c_x > \sim$50 m s^{-1}) than in 2022. Thus, the eastward acceleration due to the eastward wave breaking above $z = \sim$65 km that prevents the westward acceleration by westward waves is weaker in 2023. This is one of the plausible causes for the strong easterly winds above $z = 80$ km in 2023.

Similarly, the enhanced strength of the westerly wind at $z = \sim$65 km in 2023 is likely attributable to the strong easterly wind at $z = \sim$42 km in March. This easterly wind prevents upward propagation of westward waves that can cause westward acceleration through wave breaking above. Thus, the eastward acceleration above 42 km is expected to be stronger in 2023.

The strong easterly winds at $z = \sim$42 km in March 2023 may be linked to the stratospheric QBO phase, which is westerly (easterly) at $z = \sim$25 km in 2023 (2022). In 2023, all waves with negative c_x, which facilitate westward acceleration, can reach $z = \sim$42 km and the range of positive c_x, waves with which prevent westward acceleration above, is narrower than in 2022. Notably, there is a clear relation between the QBO and diurnal tide amplitude (e.g., Garcia, 2023). While a detailed analysis of QBO effects on tides in the upper atmosphere using the full JAWARA reanalysis is possible, it is beyond this paper's scope due to space limitations.

4. Summary and Concluding Remarks

The JAWARA reanalysis, which encompasses the entire neutral atmosphere from the ground to the lower thermosphere, has been employed to examine the formation mechanism of a strong easterly wind event (~−80 m s^{-1}) observed at $z = 80$–90 km in the upper equatorial mesosphere around the March equinox of 2023. To understand this mechanism, the dynamical conditions for 2023 and 2022 during the March equinox were compared.

10.1029/2025GL114658

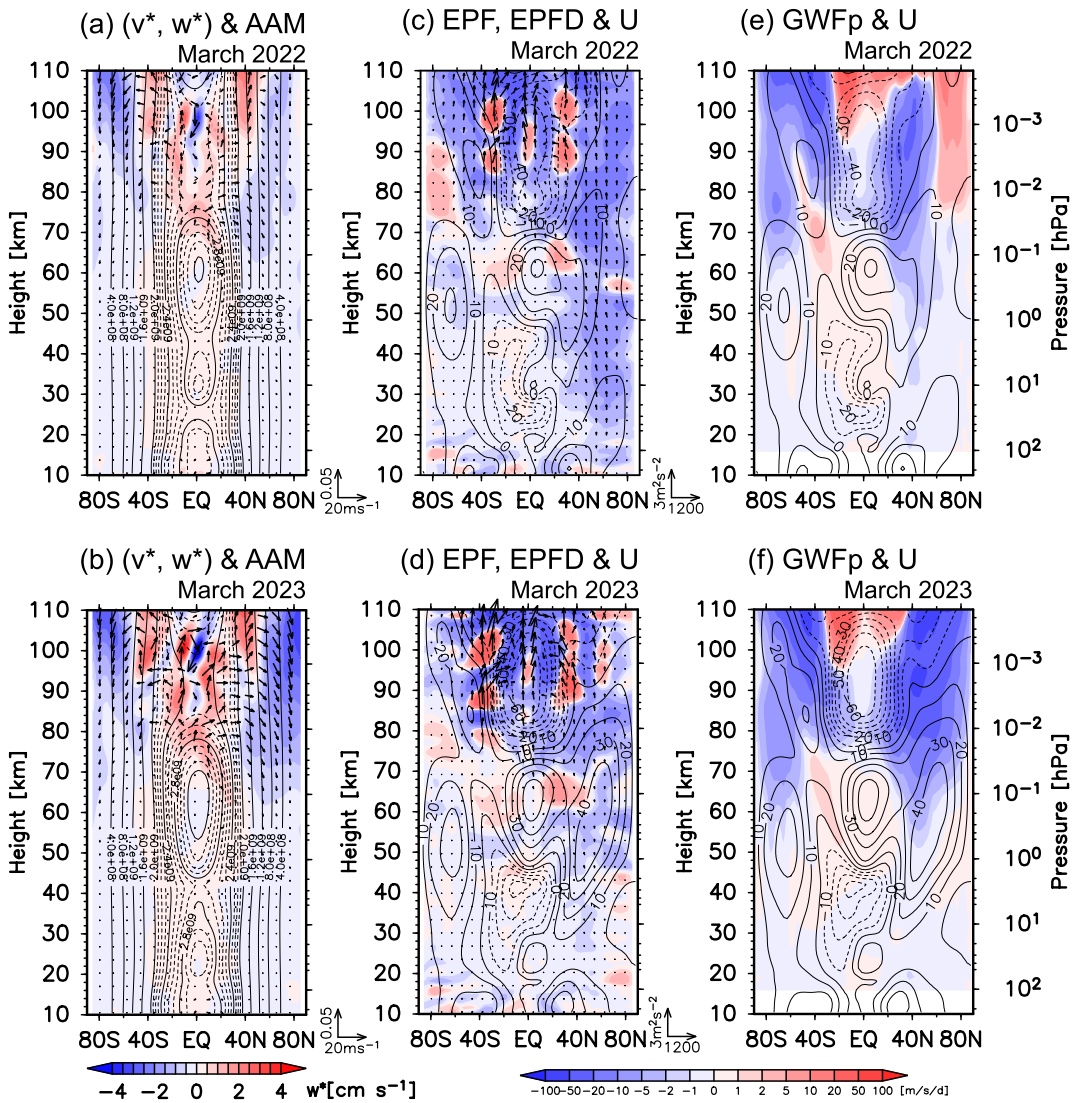

Figure 3. Meridional cross section of the angular momentum (contours), the residual mean flow (arrows), and its vertical component (colors) in (a) 2022 and (b) 2023. (c, d): The same as (a, b) but for the zonal mean zonal wind (contours), E-P flux (arrows), and EPFD (colors). (e, f): The same as (c, d) but for parameterized gravity wave forcing (colors).

A momentum budget analysis indicates significant westward acceleration due to GWFp at $z = 82$ km, observed only in 2023. The total wave forcing is more than four times greater than the negative zonal wind tendency. However, the eastward wind advection by residual upward flows in the strong easterly shear dominated the wave forcing, suggesting the existence of another large westward acceleration mechanism, although it is partly due to a lack of assimilated observation data in the upper mesosphere. One of the plausible candidates for this mechanism is the wave forcing that is not represented by the GW parameterizations. Such strong wave forcing is likely associated with the breaking of waves interacting with the distinctive mean zonal flow observed below $z = 82$ km, including strong S-SAO westerly winds and the QBO westerly phase. Such characteristic mean wind structure is not observed in 2022.

In the future, it is essential to conduct a comprehensive investigation into the relation between the pronounced easterly wind during the March equinox in the upper mesosphere and the QBO utilizing the long-term data. Moreover, examining the energy sources of upward propagating waves, such as their connection to ENSO, is important. Quantitative research using JAWARA will enhance understanding of the characteristics and mechanisms of the mesospheric QBO as suggested by previous studies (e.g., Baldwin et al., 2001).

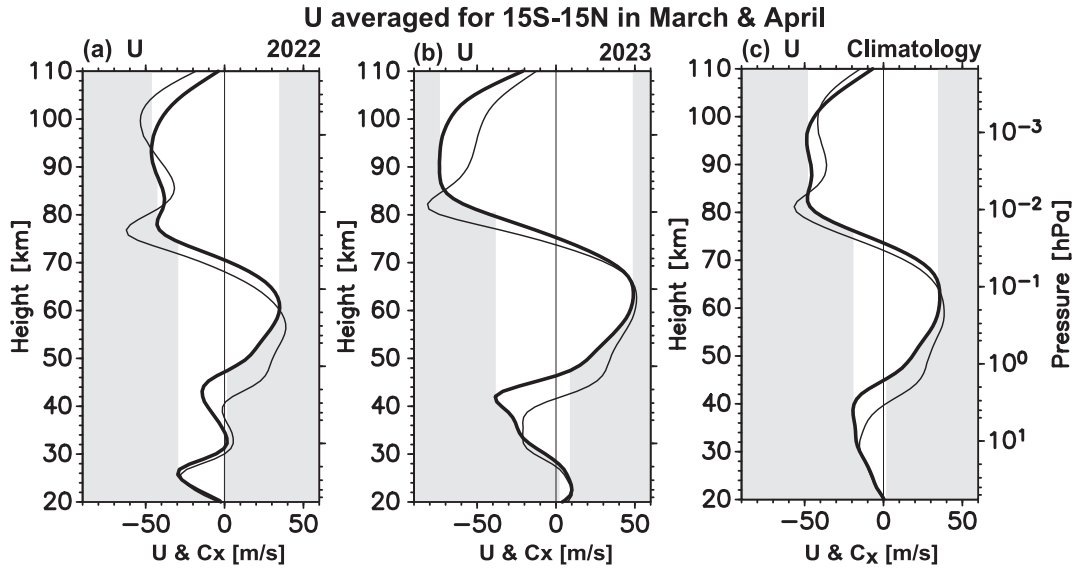

Figure 4. Vertical profiles of the zonal mean zonal wind in March (thick curves) and April (thin curves) averaged over 15°S–15°N in (a) 2022, (b) 2023, and (c) climatology for 2005–2023. Shaded regions indicate the zonal phase speed of waves that do not reach their critical level while propagating upward from 20 km just above the tropopause.

Data Availability Statement

The JAWARA data set is available at https://jawara.nipr.ac.jp. The processed JAWARA data are available at https://pansy.eps.s.u-tokyo.ac.jp/archive_data/Sato_etal_EEWE_2025/ in PANSY—Research Data Repository with CC-BY 4.0. The original radar data is available in Suclupe (2024).

Acknowledgments

We appreciate constructive comments by Kevin Hamilton, Yosuke Yamazaki, and an anonymous reviewer. This study was supported by the JSPS KAKENHI Grants JP22H00169 (KS). DK is supported by JSPS Overseas Research Fellowships. JAWARA was produced with the Earth Simulator at JAMSTEC. The S. J. do Cariri meteor radar is operated by Observatório de Luminescência Atmosférica da Paraíba (OLAP) UFCG from collaboration with INPE. This research was partially supported by ISSI in Bern and Beijing, through Projects ISSI 23-571 and ISSI-BJ 59.

References

Andrews, D. G., Holton, J. R., & Leovy, C. B. (1987). *Middle atmosphere dynamics (No. 40)*. Academic Press.

Antonita, T. M., Ramkumar, G., Kumar, K. K., & Deepa, V. (2008). Meteor wind radar observations of GW momentum fluxes and their forcing toward the mesospheric semiannual oscillation. *Journal of Geophysical Research*, *113*(D10), D10115. https://doi.org/10.1029/2007jd009089

Baldwin, M. P., Gray, L. J., Dunkerton, T. J., Hamilton, K., Haynes, P. H., Randel, W. J., et al. (2001). The quasi-biennial oscillation. *Reviews of Geophysics*, *39*(2), 179–229. https://doi.org/10.1029/1999RG000073

Buriti, R. A., Hocking, W. K., Batista, P. P., Medeiros, A. F., & Clemesha, B. R. (2008). Observations of equatorial mesospheric winds over Cariri (7.4°S) by a meteor radar and comparison with existing models. *Annales Geophysicae*, *26*(3), 485–497. https://doi.org/10.5194/angeo-26-485-2008

Chau, J. L., Urco, J. M., Vierinen, J., Harding, B. J., Clahsen, M., Pfeffer, N., et al. (2021). Multistatic specular meteor radar network in Peru: System description and initial results. *Earth and Space Science*, *8*(1), e01293. https://doi.org/10.1029/2020EA001293

Conte, J. F., Chau, J. L., Yiğit, E., Suclupe, J., & Rodríguez, R. (2023). Investigation of mesosphere and lower thermosphere dynamics over central and northern Peru using SIMONe systems. *Journal of the Atmospheric Sciences*, *81*(1), 93–104. https://doi.org/10.1175/jas-d-23-0030.1

Delisi, D. P., & Dunkerton, T. J. (1988). Seasonal variation of the semiannual oscillation. *Journal of the Atmospheric Sciences*, *45*(19), 2772–2787. https://doi.org/10.1175/1520-0469(1988)045<2772:SVOTSO>2.0.CO;2

Ern, M., Diallo, M., Preusse, P., Mlynczak, M. G., Schwartz, M. J., Wu, Q., & Riese, M. (2021). The semiannual oscillation (SAO) in the tropical middle atmosphere and its gravity wave driving in reanalyses and satellite observations. *Atmospheric Chemistry and Physics*, *21*(18), 13763–13795. https://doi.org/10.5194/acp-21-13763-2021

Garcia, R. R. (2023). On the structure and variability of the migrating diurnal temperature tide observed by SABER. *Journal of the Atmospheric Sciences*, *80*(3), 687–704. https://doi.org/10.1175/JAS-D-22-0167.1

Garcia, R. R., Dunkerton, T. J., Lieberman, R. S., & Vincent, R. A. (1997). Climatology of the semiannual oscillation of the tropical middle atmosphere. *Journal of Geophysical Research*, *102*(22), 19–26. https://doi.org/10.1029/97jd00207

Gray, L. J., Lu, H., Brown, M. J., Knight, J. R., & Andrews, M. B. (2022). Mechanisms of influence of the Semi-Annual Oscillation on stratospheric sudden warmings. *Quarterly Journal of the Royal Meteorological Society*, *148*(744), 1223–1241. https://doi.org/10.1002/qj.4256

Hirota, I. (1978). Equatorial waves in the upper stratosphere and mesosphere in relation to the semiannual oscillation of the zonal wind. *Journal of the Atmospheric Sciences*, *35*(4), 714–722. https://doi.org/10.1175/1520-0469(1978)035<0714:ewitus>2.0.co;2

Hitchman, M. H., & Leovy, C. B. (1988). Estimation of the Kelvin wave contribution to the semiannual oscillation. *Journal of the Atmospheric Sciences*, *45*(9), 1462–1475. https://doi.org/10.1175/1520-0469(1988)045<1462:EOTKWC>2.0.CO;2

Holton, J. R., & Wehrbein, W. M. (1980). A numerical model of the zonal mean circulation of the middle atmosphere. *PAGEOPH*, *118*(1), 284–306. https://doi.org/10.1007/BF01586455

Kawatani, Y., Hirooka, T., Hamilton, K., Smith, A. K., & Fujiwara, M. (2020). Representation of the equatorial stratopause semiannual oscillation in global atmospheric reanalyses. *Atmospheric Chemistry and Physics*, *20*(14), 9115–9133. https://doi.org/10.5194/acp-20-9115-2020

Kim, Y.-H., Voelker, G. S., Bölöni, G., Zängl, G., & Achatz, U. (2024). Crucial role of obliquely propagating gravity waves in the quasi-biennial oscillation dynamics. *Atmospheric Chemistry and Physics*, *24*(5), 3297–3308. https://doi.org/10.5194/acp-24-3297-2024

Koshin, D., Sato, K., Kohma, M., & Watanabe, S. (2022). An update on the 4D-LETKF data assimilation system for the whole neutral atmosphere. *Geoscientific Model Development*, *15*(5), 2293–2307. https://doi.org/10.5194/gmd-15-2293-2022

Koshin, D., Sato, K., Miyazaki, K., & Watanabe, S. (2020). An ensemble Kalman filter data assimilation system for the whole neutral atmosphere. *Geoscientific Model Development*, *13*(7), 3145–3177. https://doi.org/10.5194/gmd-13-3145-2020

Koshin, D., Sato, K., Wanabe, S., & Miyazaki, K. (2025). The JAGUAR-DAS whole neutral atmosphere reanalysis: JAWARA. *Progress in Earth and Planetary Science*, *12*, 1. https://doi.org/10.1186/s40645-024-00674-3

Lindzen, R. S. (1981). Turbulence and stress owing to gravity wave and tidal breakdown. *Journal of Geophysical Research*, *86*(C10), 9707–9714. https://doi.org/10.1029/JC086iC10p09707

McCormack, J. P., Harvey, V. L., Randall, C. E., Pedatella, N., Koshin, D., Sato, K., et al. (2021). Intercomparison of middle atmospheric meteorological analyses for the northern hemisphere winter 2009-2010. *Atmospheric Chemistry and Physics*, *21*(23), 17577–17605. https://doi.org/10.5194/acp-21-17577-2021

Poblet, F. L., Chau, J. L., Conte, J. F., Vierinen, J., Suclupe, J., Liu, A. Z., & Rodriguez, R. R. (2023). Extreme horizontal wind perturbations in the mesosphere and lower thermosphere over South America associated with the 2022 Hunga Eruption. *Geophysical Research Letters*, *50*(12), e2023GL103809. https://doi.org/10.1029/2023GL103809

Rao, S. V. B., Eswaraiah, S., Venkat Ratnam, M., Kosalendra, E., Kishore Kumar, K., Sathish Kumar, S., et al. (2014). Advanced meteor radar installed at Tirupati: System details and comparison with different radars. *Journal of Geophysical Research*, *119*(21), 11893–11904. https://doi.org/10.1002/2014JD021781

Ray, E. A., Alexander, M. J., & Holton, J. R. (1998). An analysis of the structure and forcing of the equatorial semiannual oscillation in zonal wind. *Journal of Geophysical Research*, *103*(D2), 1759–1774. https://doi.org/10.1029/97JD02679

Reed, R. J. (1966). Zonal wind behavior in the equatorial stratosphere and lower mesosphere. *Journal of Geophysical Research*, *71*(18), 4223–4233. https://doi.org/10.1029/jz071i018p04223

Sato, K. (2025). JAGUAR data assimilation system whole neutral atmosphere reanalysis (JAWARA) [Dataset]. https://doi.org/10.17592/002.2025010407

Sato, K., & Hirano, S. (2019). The climatology of Brewer-Dobson circulation and the contribution of gravity waves. *Atmospheric Chemistry and Physics*, *19*(7), 4517–4539. https://doi.org/10.5194/acp-19-4517-2019

Sato, K., Tateno, S., Watanabe, S., & Kawatani, Y. (2012). Gravity wave characteristics in the Southern Hemisphere revealed by a high-resolution middle-atmosphere general circulation model. *Journal of the Atmospheric Sciences*, *69*(4), 1378–1396. https://doi.org/10.1175/JAS-D-11-0101.1

Sato, K., Watanabe, S., Kawatani, Y., Tomikawa, Y., Miyazaki, K., & Takahashi, M. (2009). On the origins of mesospheric gravity waves. *Geophysical Research Letters*, *36*(19), L19801. https://doi.org/10.1029/2009GL039908

Smith, A. K., Garcia, R. R., Moss, A. C., & Mitchell, N. J. (2017). The semiannual oscillation of the tropical zonal wind in the middle atmosphere derived from satellite geopotential height retrievals. *Journal of the Atmospheric Sciences*, *74*(8), 2413–2425. https://doi.org/10.1175/JAS-D-17-0067.1

Smith, A. K., Holt, L. A., Garcia, R. R., Anstey, J. A., Serva, F., Butchart, N., et al. (2020). The equatorial stratospheric semiannual oscillation and time-mean winds in QBOi models. *Quarterly Journal of the Royal Meteorological Society*, *148*(744), 1593–1609. https://doi.org/10.1002/qj.3690

Smith, A. K., Lesley, J. G. J., & García, R. R. (2023). Evidence for the influence of the quasi-biennial oscillation on the semiannual oscillation in the tropical middle atmosphere. *Journal of the Atmospheric Sciences*, *80*(7), 1755–1769. https://doi.org/10.1175/JAS-D-22-0255.1

Suclupe, J. (2024). SuclupeGRL2024 [Dataset]. *Leibniz Institute of Atmospheric Physics at the University of Rostock*. https://doi.org/10.22000/GJDVNFGQBXFGOSUQ

Suclupe, J., Chau, J. L., Conte, J. F., Milla, M., Pedatella, N. M., & Kuyeng, K. (2023). Climatology of mesosphere and lower thermosphere diurnal tides over Jicamarca (12°S, 77°W): Observations and simulations. *Earth Planets and Space*, *75*(1), 186. https://doi.org/10.1186/s40623-023-01935-z

Suclupe, J., Chau, J. L., Conte, J. F., Pedatella, N. M., Garcia, R., Sato, K., et al. (2024). On the abnormally strong westward phase of the mesospheric semiannual oscillation at low latitudes during March equinox 2023. *Geophysical Research Letters*, *51*(16), e2024GL110331. https://doi.org/10.1029/2024GL110331

Tomikawa, Y., Sato, K., Watanabe, S., Kawatani, Y., Miyazaki, K., & Takahashi, M. (2008). Wintertime temperature maximum at the subtropical stratopause in a T213l256 GCM. *Journal of Geophysical Research*, *113*(D17), D17117. https://doi.org/10.1029/2008jd009786

Vadas, S. L., Zhao, J., Chu, X., & Becker, E. (2018). The excitation of secondary gravity waves from local body forces: Theory and observation. *Journal of Geophysical Research: Atmospheres*, *123*(17), 9296–9325. https://doi.org/10.1029/2017JD027970

Wang, Y., Li, G., Ning, B., Yang, S., Sun, W., & Yu, Y. (2019). All-sky interferometric meteor radar observations of zonal structure and drifts of low-latitude ionospheric E region irregularities. *Earth and Space Science*, *6*(12), 2653–2662. https://doi.org/10.1029/2019EA000884